

Noise measurements at seismic array in the drilling site of Bagnolifutura, Campi Flegrei

Quaderni di Geofisica



111



Istituto Nazionale di
Geofisica e Vulcanologia

Quaderni di Geofisica

Direttore

Enzo Boschi

Editorial Board

Raffaele Azzaro (CT)

Sara Barsotti (PI)

Mario Castellano (NA)

Viviana Castelli (BO)

Rosa Anna Corsaro (CT)

Luigi Cucci (RM1)

Mauro Di Vito (NA)

Marcello Liotta (PA)

Simona Masina (BO)

Mario Mattia (CT)

Nicola Pagliuca (RM1)

Umberto Sciacca (RM1)

Salvatore Stramondo (CNT)

Andrea Tertulliani - Editor in Chief (RM1)

Aldo Winkler (RM2)

Gaetano Zonno (MI)

Segreteria di Redazione

Francesca Di Stefano - coordinatore

Tel. +39 06 51860068

Fax +39 06 36915617

Rossella Celi

Tel. +39 06 51860055

Fax +39 06 36915617

redazionecen@ingv.it



Noise measurements at seismic array in the drilling site of Bagnolifutura, Campi Flegrei

Misure di rumore con array sismici nel sito di Bagnolifutura, Campi Flegrei

Simona Petrosino¹, Francesca Bianco¹, Antonella Bobbio¹, Mario Castellano¹,
Paola Cusano¹, Edoardo Del Pezzo¹, Danilo Galluzzo¹, Mario La Rocca¹,
Veronica Maiello^{1,2}

¹INGV (Istituto Nazionale di Geofisica e Vulcanologia, Sezione di Napoli - Osservatorio Vesuviano)

²Università degli Studi di Napoli “Parthenope” (Facoltà di Ingegneria, Dipartimento per le Tecnologie)

Noise measurements at seismic array in the drilling site of Bagnolifutura, Campi Flegrei

In 2012 two seismic surveys were carried out in the area of Bagnolifutura (Campi Flegrei, Naples), with the aim of characterizing the properties of the seismic noise during the drilling activity performed in the framework of the Campi Flegrei Deep Drilling Project (CFDDP; <https://sites.google.com/site/cfddpproject/>). During the first survey, which was conducted from 2 to 4 April, before the drilling, seven broadband three-component seismometers were installed in two different array configurations. The second survey started on November 26, in concomitance with the drilling operations and fluid injection, and ended on December 5, four days after the end of the drilling, when the maximum depth of 502 m was reached. During this period seven broadband and one short-period three-component sensors were installed. A preliminary spectral analysis was performed on samples of seismic noise; moreover the root mean square of the amplitude of the signals and the polarization parameters were calculated. The preliminary results show similar spectral and polarization features for the data of the two surveys, whereas the amplitude of the seismic noise collected during the second survey is greatly influenced by the bad meteorological conditions. As future development experimental site transfer functions from Nakamura's technique and surface wave dispersion from array techniques will be calculated to obtain the shallow crustal structure. The results corresponding to the different phases of the drilling activity will be compared, with the aim of establishing if significant variations of the medium properties have occurred during the experiment. Moreover the recorded signals will be deeply investigated in order to detect the eventual occurrence of microseismicity induced by fluid injection and to define its features.

Nel corso del 2012 sono state realizzate due campagne di acquisizione dati nell'area di Bagnolifutura (Campi Flegrei, Napoli), con lo scopo di caratterizzare le proprietà del rumore sismico durante l'attività di perforazione avvenuta nell'ambito del progetto Campi Flegrei Deep Drilling Project (CFDDP; <https://sites.google.com/site/cfddpproject/>). Durante la prima campagna, condotta dal 2 al 4 aprile, prima della perforazione, sono stati installati sette sismometri a larga banda a tre componenti, in due diverse configurazioni di array. La seconda campagna è iniziata il 26 novembre, in concomitanza con le operazioni di perforazione e l'iniezione di fluidi, e si è conclusa il 5 dicembre, quattro giorni dopo la fine della perforazione che ha raggiunto la massima profondità di 502 m. In questo periodo sono stati installati sette sensori a larga banda ed uno a corto periodo, tutti a tre componenti. È stata effettuata un'analisi spettrale preliminare sui campioni di rumore sismico; inoltre sono stati calcolati lo scarto quadratico medio dell'ampiezza del segnale e i parametri di polarizzazione. I risultati preliminari mostrano, per i dati registrati durante le due campagne, caratteristiche spettrali e di polarizzazione simili, mentre l'ampiezza del rumore sismico registrato durante la seconda campagna appare fortemente influenzata dalle cattive condizioni meteorologiche. Come sviluppo futuro, saranno calcolate le funzioni di trasferimento del sito mediante il metodo di Nakamura, e la dispersione delle onde superficiali attraverso le tecniche di array, con lo scopo di ottenere la struttura crostale superficiale. I risultati corrispondenti alle diverse fasi dell'attività di perforazione saranno confrontati con lo scopo di verificare se sono avvenute variazioni significative delle proprietà del mezzo nel corso dell'esperimento. Inoltre i segnali registrati saranno attentamente esaminati per rilevare l'eventuale presenza di microseismicità indotta dall'iniezione di fluidi, e per definirne le caratteristiche.

Introduction

The seismic noise can provide a great deal of information about the medium in which seismic waves propagate, therefore its analysis represents a valid tool to investigate the shallow crustal properties. Single-station techniques such as Horizontal-to-Vertical (H/V) spectral ratio [Nakamura 1989] have been widely used for the estimate of site effects [Parolai et al. 2004; Maresca et al. 2006; Bonnefoy-Claudet et al., 2009]. Moreover multichannel techniques such as Frequency-Wave number (f-k) [Lacoss et al. 1969] and Spatial Autocorrelation (SPAC) [Aki 1957; Bettig et al. 2001] have been applied to microtremor for retrieving the dispersion of surface waves, whose inversion can constrain shallow shear-wave velocities with a minimum level of uncertainty [Di Giulio et al, 2006; Mora et al. 2006]. Joint approaches combining all these methods [Picozzi et al. 2005; Claproot et al. 2012] with a polarization analysis [Jurkevics 1988] have revealed very powerful in determining the shallow crustal structure at fine resolution scale [Petrosino et al. 2012].

One of the great advantages in using the seismic noise for seismological studies is related to the easiness and speed of its acquisition. Moreover, the use of simple deployments such as small arrays of seismometers can provide good quality data without expensive installation costs. The drilling of a pilot hole in the framework of the Campi Flegrei Deep Drilling Project (CFDDP; <https://sites.google.com/site/cfddpproject/>) give us the opportunity to plan a parallel experiment during the different phases of the coring, aimed at the acquisition and analysis of the seismic noise by means of array techniques. Seismic arrays were installed during two surveys carried out from 2 to 4 April (April survey) and from November 26 to December 5 (November survey), 2012, in an area encompassed by the eastern border of the Campi

Flegrei caldera, western to the city of Naples. This site, where the ILVA steel mill was located, is now known as Bagnolifutura and has been selected for the realization of the pilot hole down to a depth of 502 m. The purpose of the April survey was to characterize the background properties of the seismic noise, and evaluate local site effects and the shallow velocity structure before any drilling operation took place. The second survey aimed at comparing the new data with those previously acquired, in order to evidence eventual variations of the medium properties related to the drilling and/or the fluid injection performed during the CFDDP experiment. In this way we will be able to track the temporal evolution of the shear-wave velocity structure retrieved by the joint analysis of surface wave dispersion and H/V spectral ratio, and compare it with detailed geo-mineralogical, petrological and geophysical information collected during the coring. A further aim of the surveys is the identification in the background signals of microseismic events eventually induced by the drilling and/or fluid injection. It is known that hydraulic fracturing can generate seismicity as shown by several authors [Cuenot et al. 2008; Kwiatek et al. 2010]. For this analysis, we will apply array techniques which are particularly suitable for the discrimination and the characterization of coherent signals masked in the background noise [Rost and Thomas 2002], and have been widely employed for retrieving the kinematic properties of the seismic wavefield [Almendros et al., 2007; La Rocca et al. 2010; Cros et al. 2011].

In this paper we give a detailed description of the two surveys, and show the results of the preliminary analysis of the seismic noise (spectral features, temporal distribution of the amplitude of the signal, spatial properties of the polarization vector), which provide the basis for future studies.

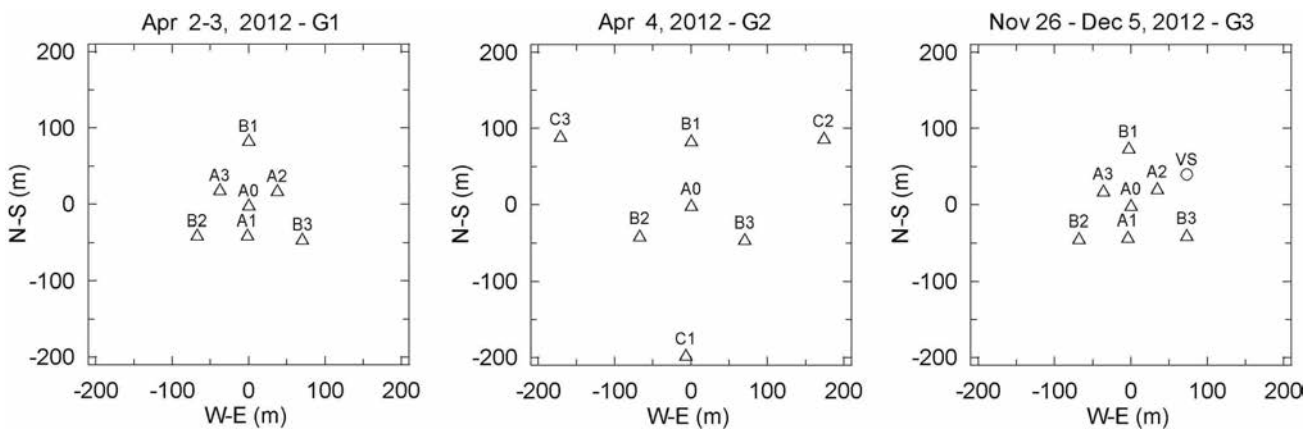


Figure 1 Seismic array configurations. From left to right, the deployments of April (G1 and G2) and November (G3) are shown. Triangles and circle represent broadband and short-period seismometers, respectively.

Figura 1 Configurazioni degli array sismici. Da sinistra verso destra, sono mostrate le geometrie di aprile (G1 e G2) e novembre (G3). I triangoli rappresentano sismometri a larga banda, il cerchio rappresenta il sensore a corto periodo.

Site Name	LAT	LON	Radius (m)	Station	Seismometer	Sampling (Hz)
A0	40.810590	14.173750	-	Reftek 130-01	LE-3D/20s	125
A1	40.810239	14.173738	39	Reftek 130-01	LE-3D/20s	125
A2	40.810765	14.174191	42	Lennartz MARSLite	LE-3D/20s	125
A3	40.810769	14.173297	43	Lennartz MARSLite	LE-3D/20s	125
B1	40.811356	14.173740	85	Lennartz MARSLite	LE-3D/20s	125
B2	40.810233	14.172954	78	Lennartz MARSLite	LE-3D/20s	125
B3	40.810200	14.174589	83	Lennartz MARSLite	LE-3D/20s	125

Table 1 Sensor code, geographic coordinates, deployed instruments and sampling rate for the G1 configuration.

Tabella 1 Codice del sensore, coordinate geografiche, strumentazione installata e frequenza di campionamento per la configurazione G1.

Site Name	LAT	LON	Radius (m)	Station	Seismometer	Sampling (Hz)
A0	40.810590	14.173750	-	Reftek 130-01	LE-3D/20s	125
B1	40.811356	14.173740	85	Lennartz MARSLite	LE-3D/20s	125
B2	40.810233	14.172954	78	Reftek 130-01	LE-3D/20s	125
B3	40.810200	14.174589	83	Lennartz MARSLite	LE-3D/20s	125
C1	40.808825	14.173691	196	Lennartz MARSLite	LE-3D/20s	125
C2	40.811402	14.175799	109	Lennartz MARSLite	LE-3D/20s	125
C3	40.811396	14.171709	107	Lennartz MARSLite	LE-3D/20s	125

Table 2 Sensor code, geographic coordinates, deployed instruments and sampling rate for the G2 configuration

Tabella 2 Codice del sensore, coordinate geografiche, strumentazione installata e frequenza di campionamento per la configurazione G2.

Site Name	LAT	LON	Radius (m)	Station	Seismometer	Sampling (Hz)
A0	40.810710	14.173840	-	Nanometrics Taurus	LE-3D/20s	100
A1	40.810340	14.173789	41	Nanometrics Taurus/Tident	LE-3D/20s	100
A2	40.810910	14.174248	41	Lennartz M24	LE-3D/20s	125
A3	40.810882	14.173414	41	Lennartz MARSLite	LE-3D/20s	125
B1	40.811388	14.173809	75	Lennartz MARSLite	LE-3D/20s	125
B2	40.810328	14.173033	80	Nanometrics Taurus	LE-3D/20s	100
B3	40.810361	14.174707	83	Lennartz MARSLite	LE-3D/20s	125
VS	40.811065	14.174707	-	Lennartz M24	LE3D-lite	125

Table 3 Sensor code, geographic coordinates, deployed instruments and sampling rate for the G3 configuration.

Tabella 3 Codice del sensore, coordinate geografiche, strumentazione installata e frequenza di campionamento per la configurazione G3.

1. Instruments and data

During the April survey, we used five Lennartz MARSLite and one Reftek 130-01 digital seismic stations, and seven broadband three-component Lennartz seismometers (LE-3D/20s). We installed seismic arrays with a circular geometry (Figure 1) in a flat area at about 50 m asl. On April 2 and 3, one sensor (A0) was placed at the center, three sensors (A1, A2 and A3) at fixed radius of about 40 m (subarray A) and the remaining three (B1, B2 and B3) at radius of about 80 m (subarray B); we will call this deployment “Configuration 1”, (G1). The sensors belonging to the same radius were evenly spaced (120°). On April 4 we changed the configuration (“Configuration 2”, G2): the sensor A0 and the subarray B were left in the same position, while sensors in A1, A2 and A3 were moved, at radius of about 200 m, to sites C1, C2 and C3 creating subarray C. The seismometer installed at B1 site was affected by a malfunction during the first two days of the survey; it was replaced on April 4. Each day about 4-5 hours of seismic noise were recorded.

An array deployment (Figure 1) similar to the G1 was set up from November 26 to December 5, using the same seven broadband seismometers; moreover a short period (1 Hz) three-component Lennartz LE3D-lite seismometer (VS) at a distance of about 40 m from A2 site, along the direction of the fence delimiting the drilling area was added (‘Configuration 3’, G3). This short period sensor was a redundant device in case of malfunction of the other seismometers; probably it will not be used for future array analysis because we prefer data from homogeneous broadband instruments. The seismic noise was continuously recorded by three Lennartz MARSLite, two Nanometrics Taurus (one of them equipped with a three-channel Trident module) and one six-channel Lennartz M24 stations. Field operations consisting in instrument check and battery replacement were performed on November 29 and December 03. Sampling rates were set at 100 sps for the Nanometrics Taurus stations and at 125 Hz for all the others instruments.

In post-processing all the recorded data were re-sampled at 125 sps and converted into 1-hour-long file in SAC format (Seismic Analysis Code; <http://www.iris.edu/software/sac/>). All the information about the instruments, the geographical coordinates and the physical units of the recorded signals are stored in the file header. The technical characteristics of the devices are reported in Tables 1, 2 and 3.

For each array configuration we calculated the array transfer function (ATF) that represents the frequency-wave number spectrum in response to a vertical incident impulse [Rost and Thomas 2002]. The wavelength resolution is directly related to the geometry of the array (inter-

sensor distance and aperture) and it is estimated from the ATF pattern [Di Giulio et al. 2006; Wathelet et al. 2008]. The ATF of the G1 was calculated without the sensor B1, due to its malfunction during the first two days. For G3 we do not include the short-period sensor in the calculus of ATF, because only data from broadband seismometers will be used for the future array analysis. For each configuration the theoretical response and the corresponding resolution limits [Wathelet et al. 2008] are shown in Figure 2. The values of minimum ($k_{\min}/2$) and maximum (k_{\max}) resolvable wavelength are also reported in Table 4.

2. Preliminary analysis: the background properties of the seismic noise

The spectra of the seismic noise were calculated for 1-h-long recordings; here, as a sample, we show the results for the data recorded at the A0 seismometer on April 4 and December 2 (Figures 3 and 4). The spectral content is spread in the 0.3-15 Hz frequency band; low frequency contribution (< 1Hz) is predominant and it is higher on the horizontal components compared with the vertical one. On the contrary, the vertical component shows slightly higher spectral peaks in the 1-15 Hz band with respect to the horizontal ones. No substantial differences are detected between the spectral peaks of the recordings of April and December, except for the higher amplitude values observed during the second survey ascribable to bad weather condition, as will be shown in the following.

For all the sensors, we calculated the root mean square (RMS) of the amplitude of the seismic noise over 1-hour-long time window with no overlap, and averaged over the three components of motion. We analysed unfiltered data and signals filtered in two frequency bands, 1-5 Hz and 0.1-1 Hz. Similar noise levels characterize all the sensors; slightly higher values are observed in the 1-5 Hz band at C1 site on April 4 (Figure 5).

Array Configuration	$k_{\min}/2$ (rad/m)	k_{\max} (rad/m)
G1	0.057	0.094
G2	0.017	0.042
G3	0.040	0.096

Table 4 Values of minimum ($k_{\min}/2$) and maximum (k_{\max}) resolvable wavelength for the different array configurations.

Tabella 4 Valori della minima ($k_{\min}/2$) e massima (k_{\max}) lunghezza d’onda risolvibile per le diverse configurazioni di array.

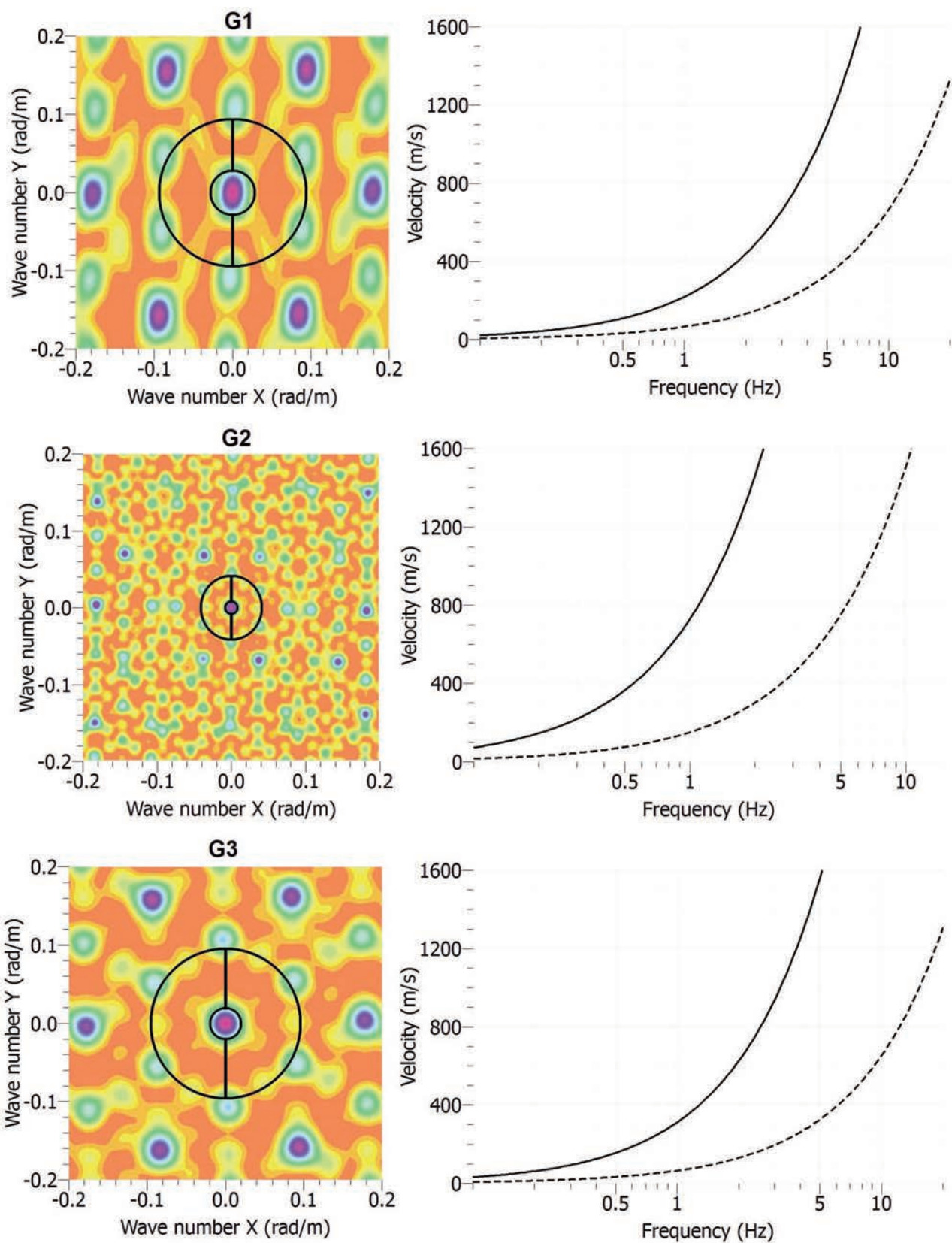


Figure 2 From the top to the bottom, array transfer function for G1, G2 and G3. The theoretical response was calculated by using the Geopsy software package available from <http://www.geopsy.org/>. For the plots on the left, the outer black circle corresponds to the alias lobe position when the magnitude of the ATF reaches a value of 0.5; this condition occurs along the direction represented by the black line. For each panel, on the right, the corresponding resolution limits are shown; solid and dot lines represent $k_{\min}/2$ and k_{\max} , respectively.

Figura 2 Dall'alto verso il basso, la funzione di trasferimento dell'array per le configurazioni G1, G2 e G3. La risposta teorica è stata calcolata usando il software Geopsy (<http://www.geopsy.org/>). Nei grafici a sinistra, il cerchio nero corrisponde al lobo di aliasing per il quale la ATF è pari a 0.5, mentre la linea nera rappresenta la direzione in cui questa condizione è verificata. Per ogni pannello, sulla destra, sono mostrati i corrispondenti limiti di risoluzione; le linee intere e tratteggiate rappresentano rispettivamente $k_{\min}/2$ e k_{\max} .

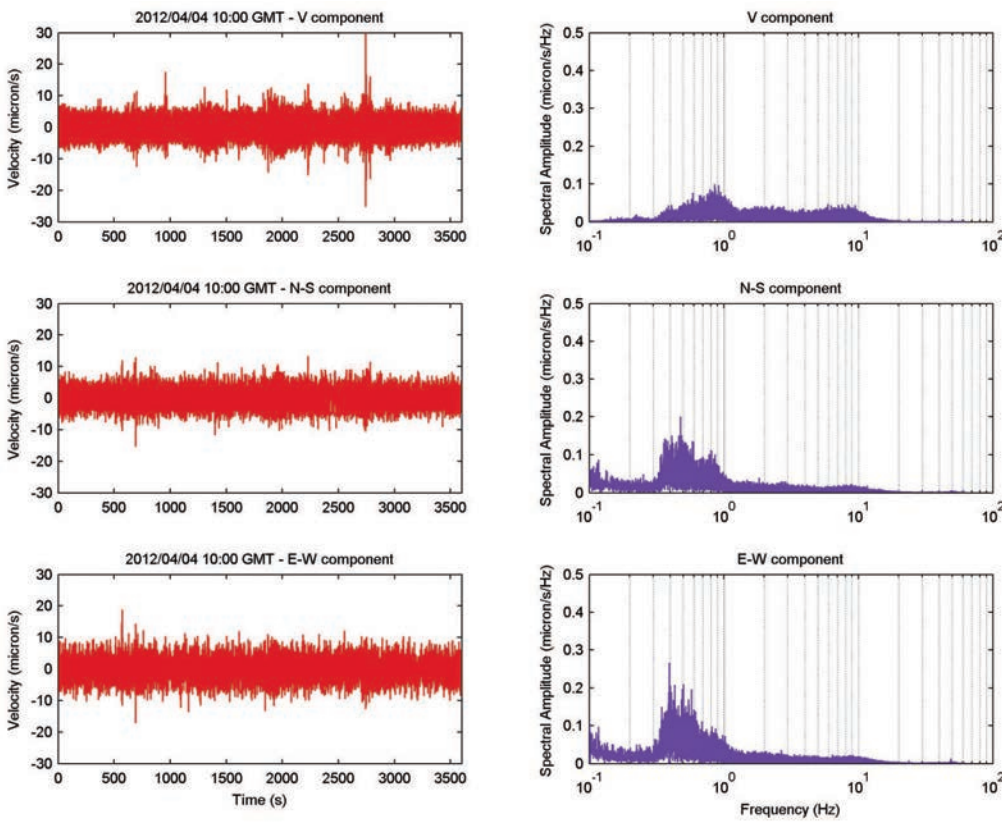


Figure 3 Three-component seismogram of 1-hour-long seismic signal recorded on April, 4, 10:00 GMT at A0 seismometer, and its amplitude spectrum.

Figura 3 Sismogramma (tre componenti) di un'ora di segnale registrato il giorno 4 aprile, ore 10:00 GMT al sismometro A0, e relativo spettro.

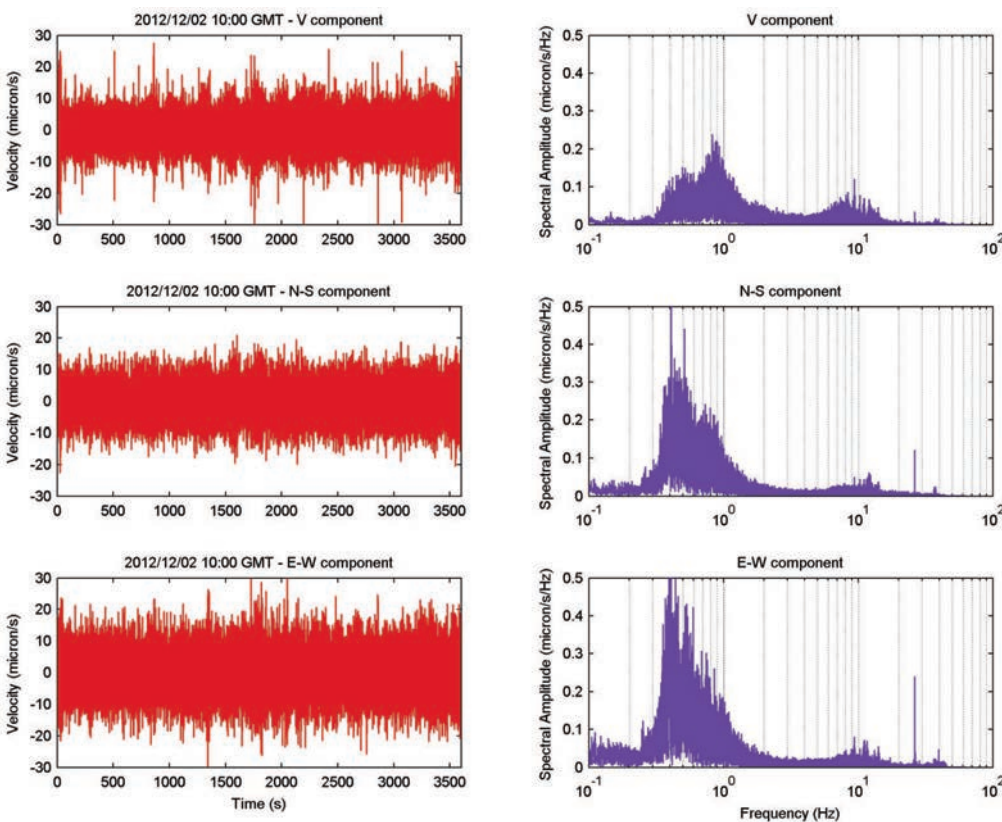


Figure 4 Three-component seismogram of 1-hour-long seismic signal recorded on December, 2, 10:00 GMT at A0 seismometer and its amplitude spectrum.

Figura 4 Sismogramma (tre componenti) di un'ora di segnale registrato il giorno 2 dicembre, ore 10:00 GMT al sismometro A0, e relativo spettro.

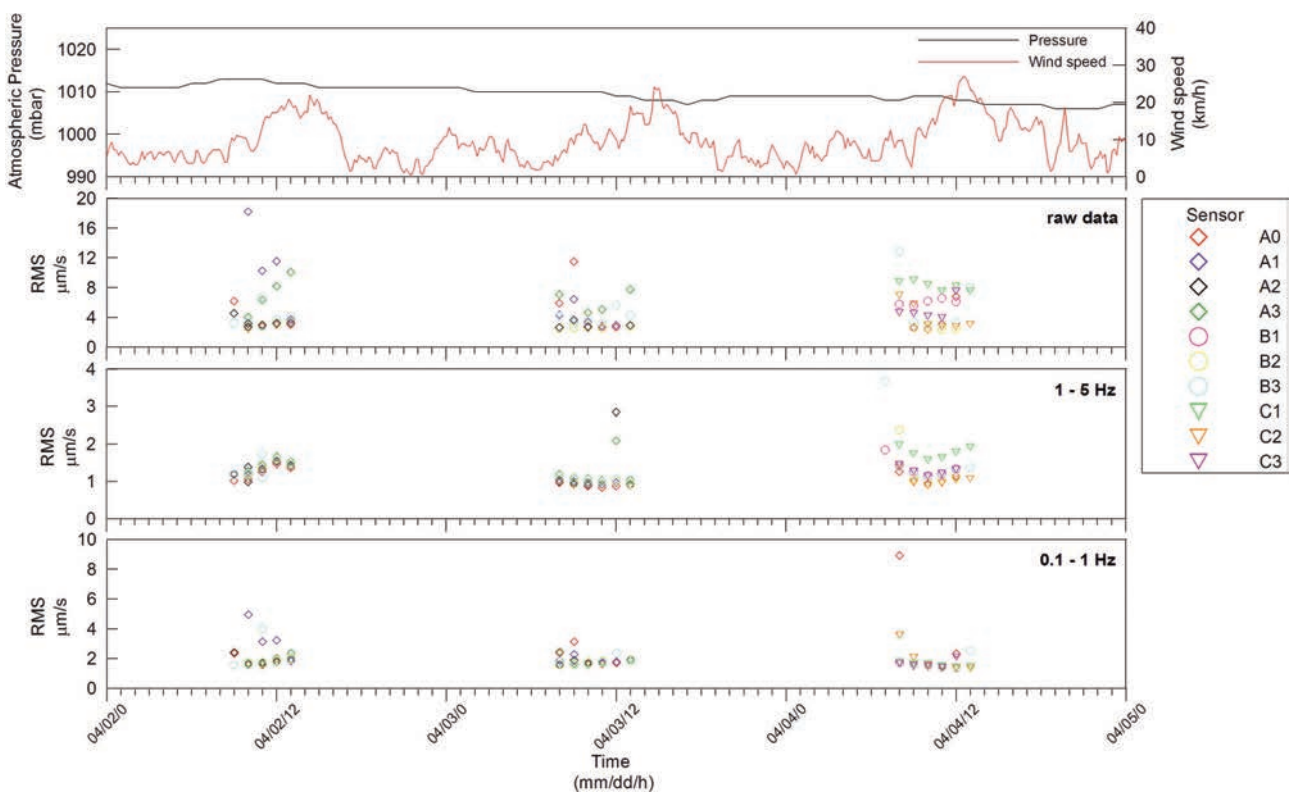


Figure 5 Temporal pattern of the meteorological data and RMS of the seismic noise recorded at all the sensors during the April survey. From top to bottom: atmospheric pressure and wind speed; unfiltered seismic data; data filtered in the 1-5 Hz frequency band; data filtered in the 0.1-1 Hz frequency band. The few outliers are related to spikes and disturbances caused by human activity which occurred in proximity of the seismometers during some field operations.

Figura 5 Andamento temporale dei parametri meteorologici e dell'RMS del rumore sismico registrato ai diversi sensori durante la campagna di aprile. Dall'alto verso il basso: pressione atmosferica e velocità del vento; dati simici non filtrati; dati filtrati nella banda 1-5 Hz; dati filtrati nella banda 0.1-1 Hz. I pochi valori che si discostano dall'andamento generale sono dovuti alla presenza di transienti/disturbi causati dall'attività umana avvenuta in prossimità dei sismometri durante alcune operazioni di campagna.

The same analysis was performed on the continuous time-record of the November survey. The 24-h periodicity of the seismic noise amplitude due to anthropogenic activity and generally observed in the 1-5 Hz frequency band [Bianco et al. 2012, Petrosino et al. 2012] in this case is masked by the effects of the bad weather condition which occurred during the days of the survey. In Figure 6 the time pattern of the RMS noise amplitude, together with the atmospheric pressure and the wind speed are shown (meteo data: <http://www.wunderground.com>); the noise and weather time series appear to be strongly correlated. The meteo-marine contribution is particularly evident in the 1-10 s band: low atmospheric pressure and high wind speed likely cause an increase in the seismic noise, thus affecting its RMS amplitude. Bad weather conditions did not cause any malfunction of the instruments, and the overall quality of the dataset remains good for the investigated period.

Finally, we made a polarization analysis of the seismic noise by applying the covariance matrix method [Jurkevics, 1988] to the three-component seismograms. The polarization parameters (azimuth, incidence angle and rectilinearity) were calculated in the 0.1-1 and 1-5 Hz frequency bands for

time windows containing two wave cycles, with an overlap of 50%. The temporal pattern was obtained by averaging the values over a 1-hour-long time window. In the 0.1-1 Hz band, the average polarization azimuth is coherent for all the array sensors and it shows a preferential orientation in the E-W direction; the average incidence angle is close to 80° - 90° . More scattered azimuth values are observed in the 1-5 Hz; in this frequency band the analysis reveals the presence of waves impinging with a polarization angle of about 45° . The spatial distribution of the polarization azimuth averaged over the whole periods of acquisition is represented by the rose plots in Figures 7 and 8 for the 0.1-1 Hz band, and Figures 9 and 10 for the 1-5 Hz band: no significant differences in the mean direction of the azimuth are observed between the April and November survey.

3. Conclusions

The results of the preliminary analysis of the data recorded during two surveys at Bagnolifutura allow us to characterize the background properties of the seismic noise. The major

contributions to the spectral content are in the typical microseism (0.1-1 Hz) and cultural (1-15 Hz) bands [Peterson, 1993]. For the November survey the RMS amplitude is strongly affected by the bad weather condition, reaching higher level than that observed during the April survey. The mean direction of the polarization azimuth does not show any particular difference between the two periods, but one must consider that the results relative to the second survey are averaged over a longer time interval (ten days). Therefore, the November dataset requires to be deeply investigated over shorter time windows (particularly in concomitance and immediately after the fluid injection) in order to evidence eventual short-term variations of the RMS amplitude and of the polarization properties, and to correlate them with the drilling operation.

As observed during the preliminary analysis, the entire dataset has a good quality and it is suitable for further studies of the recorded seismic noise. The future application of Nakamura, f-k and SPAC techniques to the data collected during the different phases of the drilling will allow us to retrieve the dynamical pattern of the shear-wave velocity structure, tracking its temporal evolution all over the investi-

tigated periods. Downhole measurements of the physical, petrological and mineralogical properties of the rocks will constrain the seismic velocity model, thus reducing the uncertainties that generally affect the inversion procedure. Finally, we will apply array techniques for a careful analysis of the seismic wavefield in order to discriminate in the background noise microseismic events induced by the drilling and/or fluid injection, and to determine their kinematic properties. The knowledge of the precise timing of the operations performed during the drilling phase, will reduce the ambiguity related to the origin of these signals, allowing to undertake this task with a low level of uncertainty.

The surveys performed at the test site of Bagnolifutura gives us the opportunity to investigate the effects of the interaction of the shallow crust with the fluids injected by a controlled source. The study we are carrying out represents a contribution towards a better comprehension of the geothermal systems, where the fluids play a fundamental role both in triggering and modulating seismicity and hydrothermal tremor, and strongly affecting the physical properties of the medium in which seismic waves propagate.

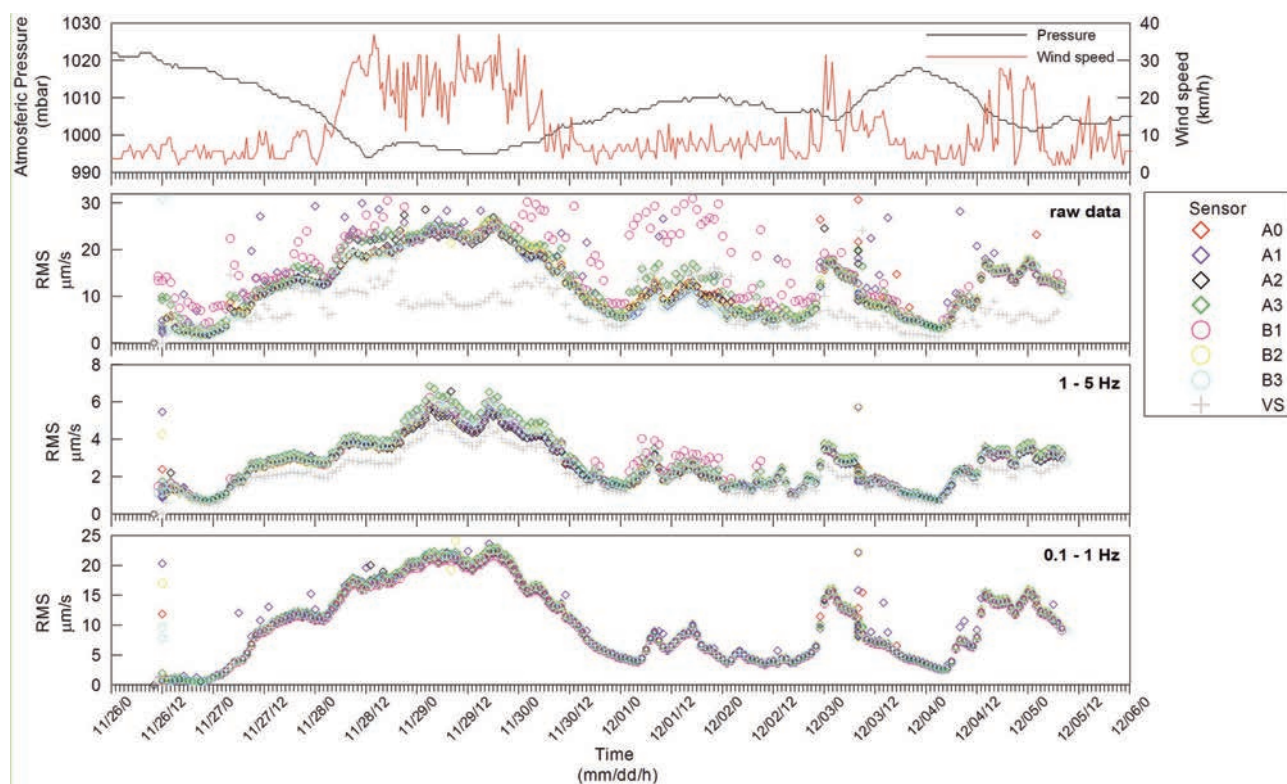


Figure 6 Temporal pattern of the meteorological data and RMS of the seismic noise recorded at all the sensors during the November survey. From top to bottom: atmospheric pressure and wind speed; unfiltered seismic data; data filtered in the 1-5 Hz frequency band; data filtered in the 0.1-1 Hz frequency band. The data of the short period sensor VS are not reported for the 0.1-1 Hz frequency band. The few outliers are related to spikes and disturbances caused by human activity which occurred in proximity of the seismometers during some field operations.

Figura 6 Andamento temporale dei parametri meteorologici e dell'RMS del rumore sismico registrato ai diversi sensori durante la campagna di novembre. Dall'alto verso il basso: pressione atmosferica e velocità del vento; dati simici non filtrati; dati filtrati nella banda 1-5 Hz; dati filtrati nella banda 0.1-1 Hz. I dati del sensore a corto periodo VS non sono riportati per la banda 0.1-1 Hz. I pochi valori che si discostano dall'andamento generale sono dovuti alla presenza di transienti/disturbi causati dall'attività umana avvenuta in prossimità dei sismometri durante alcune operazioni di campagna.



Figure 7 Rose diagrams of the polarization azimuth in the 0.1-1 Hz frequency band for data recorded during the April survey. The bins of the rose plots were chosen equal to 20° , to account for the uncertainties in the azimuth values.

Figura 7 Diagrammi a rosa dell'azimuth del vettore di polarizzazione nella banda 0.1-1 Hz per i dati registrati durante la campagna di aprile. I bins dei grafici a rosa sono pari a 20° , in accordo con le incertezze legate alla stima dei valori di azimuth.



Figure 9 Rose diagrams of the polarization azimuth in the 1-5 Hz frequency band for data recorded during the April survey. The bins of the rose plots were chosen equal to 20° , to account for the uncertainties in the azimuth values.

Figura 9 Diagrammi a rosa dell'azimuth del vettore di polarizzazione nella banda 1-5 Hz per i dati registrati durante la campagna di aprile. I bins dei grafici a rosa sono pari a 20° , in accordo con le incertezze legate alla stima dei valori di azimuth.



Figure 8 Rose diagrams of the polarization azimuth in the 0.1-1 Hz frequency band for data recorded during the November survey. The bins of the rose plots were chosen equal to 20° , to account for the uncertainties in the azimuth values. The data of the short period sensor VS are not reported for this frequency band. The green star corresponds to the location of the drill.

Figura 8 Diagrammi a rosa dell'azimuth del vettore di polarizzazione nella banda 0.1-1 Hz per i dati registrati durante la campagna di novembre. I bins dei grafici a rosa sono pari a 20° , in accordo con le incertezze legate alla stima dei valori di azimuth. I dati del sensore a corto periodo VS non sono riportati per questa banda di frequenza. La posizione della trivella è indicata dalla stella verde.



Figure 10 Rose diagrams of the polarization azimuth in the 1-5 Hz frequency band for data recorded during the November survey. The bins of the rose plots were chosen equal to 20° , to account for the uncertainties in the azimuth values. The data of the short period sensor VS are represented in yellow. The green star corresponds to the location of the drill.

Figura 10 Diagrammi a rosa dell'azimuth del vettore di polarizzazione nella banda 1-5 Hz per i dati registrati durante la campagna di novembre. I bins dei grafici a rosa sono pari a 20° , in accordo con le incertezze legate alla stima dei valori di azimuth. I dati del sensore a corto periodo VS sono rappresentati in giallo. La posizione della trivella è indicata dalla stella verde.

Acknowledgements

We wish to thank the coordinators of the CFDDP, Giuseppe De Natale and Claudia Troise, for having provided useful information about the experiment, and for the many helpful discussions and suggestions. The Administration of the Bagnolifutura S.p.A. is acknowledged for having allowed us to deploy the seismic instruments in the area. Most part of data analysis was done by using SAC (<http://www.iris.edu/software/sac/>) and Geopsy software (<http://www.geopsy.org/>). SAC, Geopsy, Google Earth was used for the base map of Figures 7, 8, 9, and 10.

References

- Aki K., (1957). *Space and time of stationary stochastic wave, with special reference to microtremors*. Bull. Earthq. Res. Ins., XXXV, 415-457.
- Almendros J., Ibáñez J.M., Carmona E. and Zandomeneghi, D., (2007). *Array analyses of volcanic earthquakes and tremor recorded at Las Cañadas caldera (Tenerife Island, Spain), during the May 2004 seismic activation of Teide volcano*. J. Volcanol. Geotherm. Res., 160, 285-299.
- Bettig B., Bard P.Y., Scherbaum F., Riepl J., Cotton F., Cornou C. and Hatzfeld D., (2001). *Analysis of dense array noise measurements using the modified spatial auto-correlation method (SPAC). Application to the Grenoble area*. Bollettino di Geofisica Teorica ed Applicata, 42, 281-304.
- Bianco F., Castellano M., Cogliano R., Cusano P., Del Pezzo E., Di Vito M.A., Fodarella A., Galluzzo D., La Rocca M., Milana G., Petrosino S., Pucillo S., Riccio G. and Rovelli A., (2010). *Caratterizzazione del noise sismico nell'area vulcanica dei Campi Flegrei (Napoli): l'esperimento "UNREST"*. Quaderni di Geofisica, 86; INGV (Ed), Roma: 21 pp. ISSN: 1590-2595.
- Bonnefoy-Claudet S., Baize S., Bonilla L. F., Berge-Thierry C., Pasten C., Campos J., Volant P. and Verdugo R., (2009). *Site effect evaluation in the basin of Santiago de Chile using ambient noise measurements*. Geophys. J. Int., 176, 925-937. doi: 10.1111/j.1365-246X.2008.04020.x
- Claprood M., Asten M. W. and Kristek J., (2012). *Combining HVSR microtremor observations with the SPAC method for site resonance study of the Tamar Valley in Launceston (Tasmania, Australia)*. Geophys. J. Int., doi: 10.1111/j.1365-246X.2012.05654.x
- Cros E., Roux P., Vandemeulebrouck J. and Kedar S., (2011). *Locating hydrothermal acoustic sources at Old Faithful Geyser using Matched Field Processing*. Geophys. J. Int., 187, 385-393. doi: 10.1111/j.1365-246X.2011.05147.x
- Cuenot N., Dorbath C. and Dorbath L., (2008). *Analysis of the Microseismicity Induced by Fluid Injections at the EGS Site of Soultz-sous-Forêts (Alsace, France): Implications for the Characterization of the Geothermal Reservoir Properties*. Pure and Applied Geophysics 165, 797-828.
- Di Giulio G., Cornou C., Ohrnberger M., Wathelet M. and Rovelli A., (2006). *Deriving Wavefield Characteristics and shear-velocity profiles from two-dimensional small-aperture arrays analysis of ambient vibrations in a small-size alluvial basin, Colfiorito, Italy*. Bull. Seismol. Soc. Am., 96, 1915-1933, doi:10.1785/0120060119.
- Jurkevics A., (1988). *Polarization analysis of three-component array data*. Bull. Seismol. Soc. Am., 78, 1725-1743.
- Lacoss R. T., Kelly E. J. and Toksoz M. N., (1969). *Estimation of seismic noise structure using array*. Geophysics, 34, 21-38, doi:10.1190/1.1439995.
- Kwiatek G., Bohnhoff M., Dresen G., Schulze A., Schulte T., Zimmermann G. and Huenges E., (2010). *Microseismicity induced during fluid-injection: A case study from the geothermal site at Groß Schönebeck, North German Basin*. Acta Geophysica, 58, 995-1020.
- La Rocca M., Galluzzo D., Malone S., McCausland W., and Del Pezzo E., (2010). *Array analysis and precise source location of deep tremor in Cascadia*. J. Geophys. Res., 115, B00A20, doi:10.1029/2008JB006041.
- Maresca R., Galluzzo D. and Del Pezzo E., (2006). *H/V spectral ratios and array techniques applied to ambient noise recorded in the Colfiorito Basin, Central Italy*. Bull. Seismol. Soc. Am., 96, 490-505, doi:10.1785/0120050057.
- Mora M., Lesage P., Valette B., Alvarado G., Leandro C., Métaxian J.-P. and Dorel J., (2006). *Shallow velocity structure and seismic site effects at Arenal volcano, Costa Rica*. J. Volcanol. Geotherm. Res., 152, 121-139, doi:10.1016/j.jvolgeores.2005.09.013.
- Nakamura Y., (1989). *A method for dynamic characteristics estimation of subsurface using microtremor on the ground surface*. Quarterly Report of Railway Technical Research Institute (RTRI), Vol. 30, No. 1.
- Parolai S., Richwalski S. M., Milkereit C. and Bormann P., (2004). *Assessment of the stability of H/V spectral ratios from ambient noise and comparison with earthquake data in the Cologne area (Germany)*. Tectonophysics, 390, 57-73. doi:10.1016/j.tecto.2004.03.024.
- Peterson J., (1993). *Observations and modeling of seismic background noise*. U.S. Geol. Surv. Open File Rep., 93-322.
- Petrosino S., Damiano N., Cusano P., Di Vito M. A., de Vita S. and Del Pezzo E., (2012). *Subsurface structure of the Solfatara volcano (Campi Flegrei caldera, Italy) as deduced from joint seismic-noise array, volcanological and morphostructural analysis*. Geochem. Geophys. Geosyst., 13, Q07006, doi:10.1029/2011GC004030.

Picozzi M., Parolai S. and Richwalski S. M., (2005). *Joint inversion of H/V ratios and dispersion curves from seismic noise: Estimating the S-wave velocity of bedrock.* Geophys. Res. Lett., 32, L11308, doi:10.1029/2005GL022878.

Rost S. and Thomas C., (2002). *Array seismology: methods and applications.* Review of Geophysics, 40, 3.

Wathelet M., Jongmans D., Ohrnberger M. and Bonnefoy-Claudet S., (2008). *Array performances for ambient vibrations on a shallow structure and consequences over Vs inversion.* J. Seismol., 12, 1–19, doi:10.1007/s10950-007-9067-x.

Index

Introduction	5
1. Instruments and data	7
2. Preliminary analysis: the background properties of seismic noise	7
3. Conclusions	10
Acknowledgements	13
References	13

Coordinamento editoriale e impaginazione
Centro Editoriale Nazionale | INGV

Progetto grafico e redazionale
Daniela Riposati | Laboratorio Grafica e Immagini | INGV

© 2013 INGV Istituto Nazionale di Geofisica e Vulcanologia
Via di Vigna Murata, 605
00143 Roma
Tel. +39 06518601 Fax +39 065041181

<http://www.ingv.it>



Istituto Nazionale di Geofisica e Vulcanologia